Journal of ELECTRONIC MATERIALS, Vol. 48, No. 6, 2019
https://doi.org/10.1007/s11664-019-07118-5

Thermoelectric Properties of Zn Doped BiCuSeO

SAYAN DAS,[1] ANBALAGAN RAMAKRISHNAN,[2] MOUMIN RUDRA,[3] KUEI-HSIEN CHEN,[2] T.P. SINHA,[3] DINESH KUMAR MISRA,[4] and RAMESH CHANDRA MALLIK [1,5]

1.—Thermoelectric Materials and Devices Laboratory, Department of Physics, Indian Institute of Science, Bangalore, India. 2.—Institute of Atomic and Molecular Sciences, Academia Sinica, No. 1, Sec. 4, Roosevelt Road, Taipei, Taiwan. 3.—Department of Physics, Bose Institute, 93/1 Acharya Prafulla Chandra Road, Kolkata 700009, India. 4.—Advanced Materials and Devices, CSIR-National Physical Laboratory, Dr KS Krishnan Marg, New Delhi 110012, India. 5.—e-mail: rcmallik@iisc.ac.in

Layered oxychalcogenide BiCuSeO is a promising thermoelectric material due to its ultra-low thermal conductivity and moderate Seebeck coefficient. The doping of monovalent/divalent elements at the Bi site helps in reducing the electrical resistivity. In this report, $Bi_{1-x}Zn_xCuSeO$ (x = 0.0, 0.02, 0.04, 0.06, 0.08, and 0.1) was prepared by the solid state synthesis to elucidate the Zn doping effect at the Bi site. Zinc oxide was used as a precursor to dope Zn at the Bi site. The x-ray diffraction patterns were matched with BiCuSeO with no additional peak, which confirms the crystal structure and phase purity of the samples. X-ray photo electron spectroscopy of the $Bi_{0.90}Zn_{0.10}CuSeO$ sample indicated a coexistence of Bi^{+3} and Bi^{+4} oxidation states. The electrical resistivity and Seebeck coefficient of the samples decreased with increase in the doping concentration because of increasing carrier concentration. The electrical resistivity of all the doped samples showed a transition from a metallic to semiconducting nature around 473 K. The Seebeck coefficient of the samples with x = 0.06, 0.08 and 0.1 showed a very weak temperature dependence above 523 K, which is a signature of small polaron hopping. The highest power factor of 0.35 mW/m K^2 was obtained for x = 0.02 at 773 K. The impedance spectroscopy of the $Bi_{0.90}Zn_{0.10}CuSeO$ sample confirmed the hopping conductivity and also the increase in the mobility of the charge carrier with temperature. The total thermal conductivity was dominated by the lattice thermal conductivity. The highest zT of 0.48 at 773 K has been obtained for x = 0.02, mainly due to the increment in the power factor.

Key words: Seebeck coefficient, electrical resistivity, thermal conductivity, small polaron

INTRODUCTION

The ever-diminishing fossil fuels and their carbon footprint have stimulated much research on clean and sustainable energy in recent times. Thermoelectricity is a promising candidate to decrease the dependence on fossil fuels, by capturing the waste heat from different sources such as exhaust of engines/generators to generate useful electricity. In spite of being scalable, noise-free and robust, thermoelectric generators have limited applications due to their low efficiency. The efficiency of thermoelectric materials is governed by the dimensionless figure of merit (zT) given as

$$zT = \frac{s^2}{\rho\kappa}T \quad (1)$$

where S is the Seebeck coefficient, ρ is the electrical resistivity, κ is the total thermal conductivity, which

(Received August 9, 2018; accepted March 7, 2019; published online March 18, 2019)

is a sum of the electronic (κ_e) and lattice part (κ_L) of the thermal conductivity, and T is the absolute temperature. To have a high-efficiency thermoelectric material, the requirements are a high Seebeck coefficient, low electrical resistivity and low thermal conductivity. High zTs (> 2) have been obtained in both p-type and n-type materials,[1,2] but stability at high temperatures in an ambient atmosphere remains a challenge. Since oxide materials are immune to oxidation at high temperatures, they can be a solution to this problem. Recently, BiCuSeO has appeared as a promising thermoelectric material, mainly relying on its ultra-low thermal conductivity. It has a layered structure with $(Bi_2O_2)^{+2}$ and $(Cu_2Se_2)^{-2}$ stacked along the c-axis. It belongs to the tetragonal crystal system with a space group of $P4/nmm$. The Bi and Se atoms take the $2c$ Wykoff position whereas O and Cu take the $2a$ and $2b$ Wykoff positions, respectively. The ultra-low thermal conductivity (< 1 W/m K) of BiCuSeO is caused by the high atomic displacement parameter of Cu, the interlayer scattering of phonons and bond anharmonicity in BiCuSeO.[3] The layered structure not only reduces the thermal conductivity, but it also enhances the Seebeck coefficient through quantum confinement. The high Seebeck coefficient of BiCuSeO is also due to the heavy hole band and one-dimensional characteristics in the density of states.[4] The main drawback of BiCuSeO as a thermoelectric material is its high electrical resistivity due to its low carrier concentration ($\sim 10^{18}$/cm^3).[5] Several strategies have been employed to reduce the electrical resistivity, such as reducing the band gap by alloying,[6,7] increasing the hole mobility by modulation doping[8] and grain alignment.[9] The direct approach to increase the carrier concentration is to create defects that can liberate holes in the system. This has been accomplished by creating Bi/Cu vacancies[5,10] or doping at the Bi site. Various elements have been doped at the Bi site such as Pb[11]; alkali metals such as Na,[12] K[13] and Cs[14]; alkaline earth metals such as Mg,[15] Ca,[16] Sr[17] and Ba[18]; and transition elements such as Ni[19] and Cd.[20]

In this report, the transition metal Zn was doped at the Bi site to increase the hole concentration and thereby improve the electrical resistivity. The mechanism of electronic conduction was determined from the impedance spectroscopy, which showed the presence of hopping conductivity in the system. The highest power factor of 0.35 mW/m K^2 was obtained at 773 K for the sample $Bi_{0.98}Zn_{0.02}CuSeO$, which is almost twice that of the pristine sample at the same temperature. Highest zT of 0.48 was found for the sample $Bi_{0.98}Zn_{0.02}CuSeO$ at 773 K, which is 65% higher than the pristine sample. The increment in the power-factor was not translated into high zT because of the increased thermal conductivity in the doped samples.

EXPERIMENTAL

Bi_2O_3 (5 N), Cu (5 N), Se (5 N) Bi (5 N) powders and ZnO nanopowder were taken in the stoichiometric ratio according to the composition $Bi_{1-x}Zn_xCuSeO$ (x = 0, 0.02, 0.04, 0.06, 0.08 and 0.10). The ZnO nanopowder was prepared using chemical precipitation.[21] All the peaks in the x-ray diffraction pattern of ZnO powder were indexed to ZnO (ICDD Card no: 70-8070) with no impurity peaks, which confirms the crystal structure and phase purity of the synthesized ZnO powder. The samples were synthesized by standard two-step solid-state synthesis, followed by ball milling and hot pressing; the details can be found elsewhere.[22] The densities of the hot pressed pellets of x = 0.0, 0.02, and 0.06 were 94% of the theoretical density, and the remaining samples were 95% of the theoretical density. X-ray diffraction (XRD) was carried out in the Rigaku Smartlab diffraction system with a Cu Kα source with a wavelength (λ) of 1.5418 Å. The Rietveld refinement of the diffraction patterns was carried out using the Fullprof software.[23] High-resolution scanning electron microscopy (SEM) on the fractured surface of the samples was carried out in FEI Sirion XL30 FEG scanning electron microscope. SEM of the polished surface of the samples was done using the FEI ESEM-Quanta 200. An AXIS ULTRA instrument was used for x-ray photoelectron spectroscopy (XPS). The Seebeck coefficient and electrical resistivity of the bar-shaped samples ($\sim 12 \times 1.8 \times 1.2$ mm^3) were measured simultaneously using the ULVAC ZEM-3 from 323 K to 773 K. The Seebeck coefficient and the electrical resistivity were measured perpendicular to the pressing direction. The impedance spectroscopy on the sample was performed from 300 K to 500 K, utilizing an LCR meter (HIOKI – 3532, Japan). A Eurotherm 818p programmable temperature controller was used to control the environment temperature with an accuracy of $\pm$ 1 K. These quantifications were performed from 42 Hz to 5 MHz frequency at the oscillation voltage of 1.0 V. Before the experiment, the flat surfaces on both sides of the pellets were cleaned properly and contacts were made by the thin silver paste. The laser flash apparatus LFA 457 MicroFlash® was used to measure thermal diffusivity (D) and the specific heat capacity (C_p) of the disk-shaped samples (diameter = 10 mm). Pyroceram was used as reference material for C_p calculations. The thermal conductivity was measured along the pressing direction. The thermal conductivity was calculated using the formula $\kappa = DdC_p$ where d is the density measured from the Archimedes principle. The error in measuring the Seebeck coefficient, electrical resistivity and thermal conductivity was 7%, 10% and 6%, respectively.

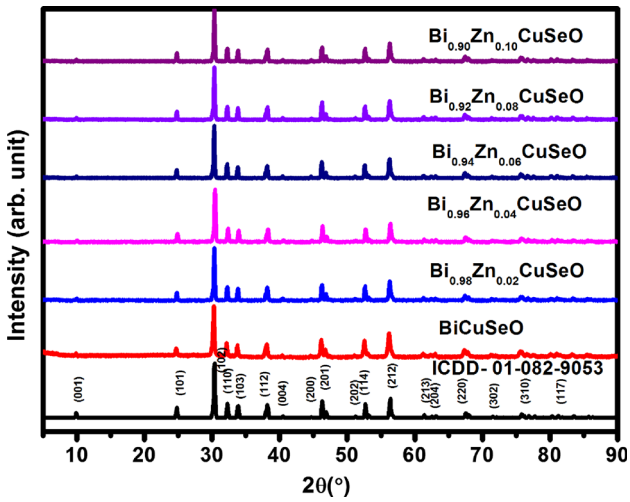

Fig. 1. X-ray diffraction pattern of the samples compared with the standard data of BiCuSeOICDD data (PDF no. 01-082-9053).

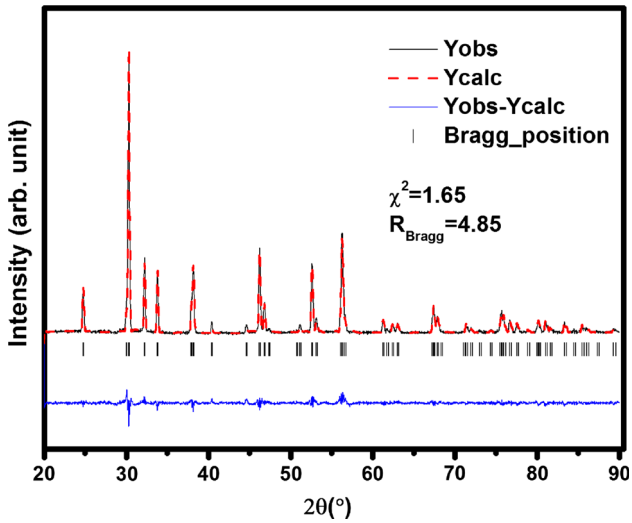

Fig. 2. The Rietveld refinement of the sample $Bi_{0.94}Zn_{0.06}CuSeO$. The continuous black line represents the experimental data; the red dashed line represents the simulated data, the blue line represents the difference between the experimental data and the simulated data. The vertical black lines represent the Bragg positions (Color figure online).

RESULTS AND DISCUSSION

X-ray Diffraction (XRD)

X-ray diffraction pattern of the samples is depicted in Fig. 1. All the peaks were matched with the standard ICDD data (PDF no. 01-082-9053) of BiCuSeO, confirming the tetragonal crystal structure with a space group of *P*4/nmm. No impurity peaks were observed in the XRD patterns, which shows that all the samples are of a single phase. The phase purity of samples indicates the high solubility of Zn at the Bi site. Rietveld refinement was performed for all the samples to refine the crystallographic information of the samples. The refinements of the powdered samples were done assuming no preferred orientation. The refinement result for $Bi_{0.98}Zn_{0.02}CuSeO$ is given in Fig. 2. The Rietveld refinement result of the other samples is given in supplementary information (see figure S1-S6). The refined lattice parameters (both *a* and *c*) from the Rietveld refinement is shown in Fig. 3. The *a* parameter does not show large variation with doping. The *c* parameter also do not show large variation with doping. Since the $(Bi_2O_2)^{+2}$ and $(Cu_2Se_2)^{-2}$ layers are coupled by Coulomb interaction, the distance between the layers (and the *c*-axis of the unit cell) is directly influenced by the charge on each layer.[24] The charge (hole) reshuffling between the layers decreases the charge on both the layers and increases the *c*-axis. Here, the *c*-axis did not change, which essentially means that the charge was not transferred from $(Bi_2O_2)^{+2}$ to the $(Cu_2Se_2)^{-2}$ layer. The Lotgering factor of the samples was calculated using the formula $L.F = \frac{P_{\text{Pellet}} - P_{\text{powder}}}{1 - P_{\text{powder}}}$, where $P = \frac{\sum I(00l)}{\sum I(hkl)}$.[25] The low Lotgering factor (≤ 0.10) along the z-axis (see supplementary table SI) shows that the pellets are isotropic and transport properties are almost similar in parallel and perpendicular to the pressing direction.

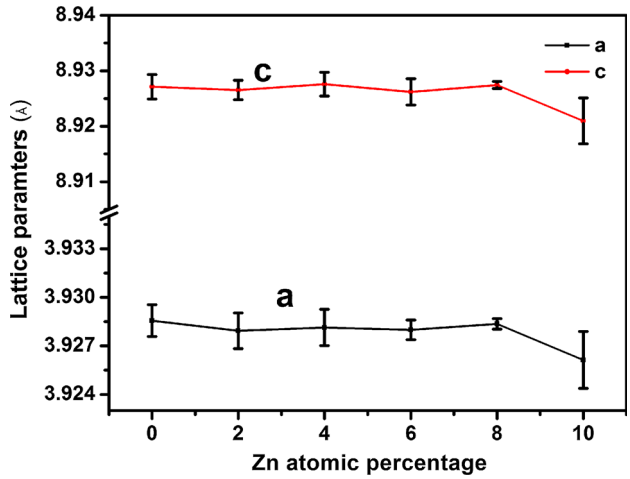

Fig. 3. Lattice parameters of the samples refined from Rietveld refinement. The square black symbol represents the "a" parameter, and red open circle symbol represents the "c" parameter (Color figure online).

Scanning Electron Microscopy (SEM)

Figure 4 shows the backscattered electron (BSE) and the corresponding secondary electron (SE) images of the polished surface of the samples. The black spots are the surface pits on the samples as shown the SE images corresponding to the BSE images. The BSE images of the polished surface of the samples do not show any secondary phase in agreement with the XRD results. Energy-dispersive x-ray spectroscopy (EDS) was performed to calculate the Bi/Cu and Cu/Zn ratio to ensure that Zn dopes at the Bi site. The results are tabulated in

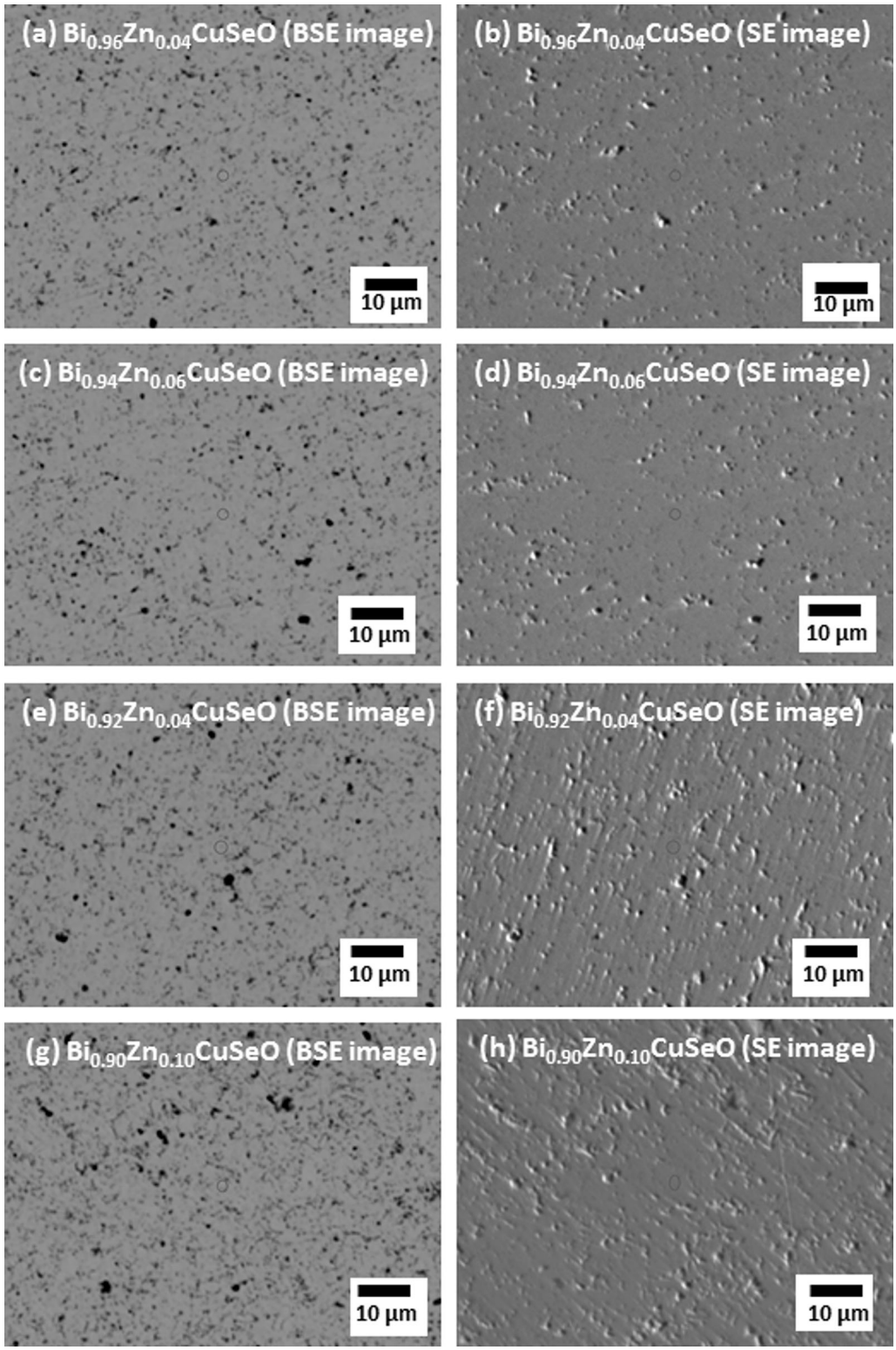

Fig. 4. Backscattered electron (BSE) image of the polished surface of (a) $Bi_{0.96}Zn_{0.04}CuSeO$ (c) $Bi_{0.94}Zn_{0.06}CuSeO$ (e) $Bi_{0.92}Zn_{0.08}CuSeO$ (g) $Bi_{0.90}Zn_{0.10}CuSeO$ and the corresponding secondary electron (SE) image of (b) $Bi_{0.96}Zn_{0.04}CuSeO$ (d) $Bi_{0.94}Zn_{0.06}CuSeO$ (f) $Bi_{0.92}Zn_{0.08}CuSeO$ (h) $Bi_{0.90}Zn_{0.10}CuSeO$.

Table I. Both the Bi/Zn and Zn/Cu ratios are close to the nominal composition, which proves that the Zn dopes at the Bi site.

The SEM images of the fractured surface of the samples are shown in Fig. 5. The particles are densely packed, indicating the high density of the

Table I. The Bi/Zn and Zn/Cu ratio of the sample obtained from energy dispersive spectroscopy (EDS)

Sample	Bi/Cu ratio	Zn/Cu ratio
$Bi_{0.98}Zn_{0.02}CuSeO$	0.975	0.031
$Bi_{0.96}Zn_{0.04}CuSeO$	0.961	0.048
$Bi_{0.94}Zn_{0.06}CuSeO$	0.947	0.068
$Bi_{0.92}Zn_{0.08}CuSeO$	0.955	0.082
$Bi_{0.90}Zn_{0.10}CuSeO$	0.906	0.091

samples. The size of the particles has a distribution of a few micrometres to less than a micrometre. The high-resolution image of the $Bi_{0.90}Zn_{0.10}CuSeO$ sample shows agglomerated particles of less than 100 nm. These sub-hundred-nanometer particles may reduce the thermal conductivity at the mid-to-low temperature ranges.[26]

X-ray Photoelectron Spectroscopy (XPS)

Figure 6 shows the x-ray photoelectron spectra of Bi 4f state of the $Bi_{0.90}Zn_{0.10}CuSeO$ sample. The binding energy of the spectrum was calibrated to

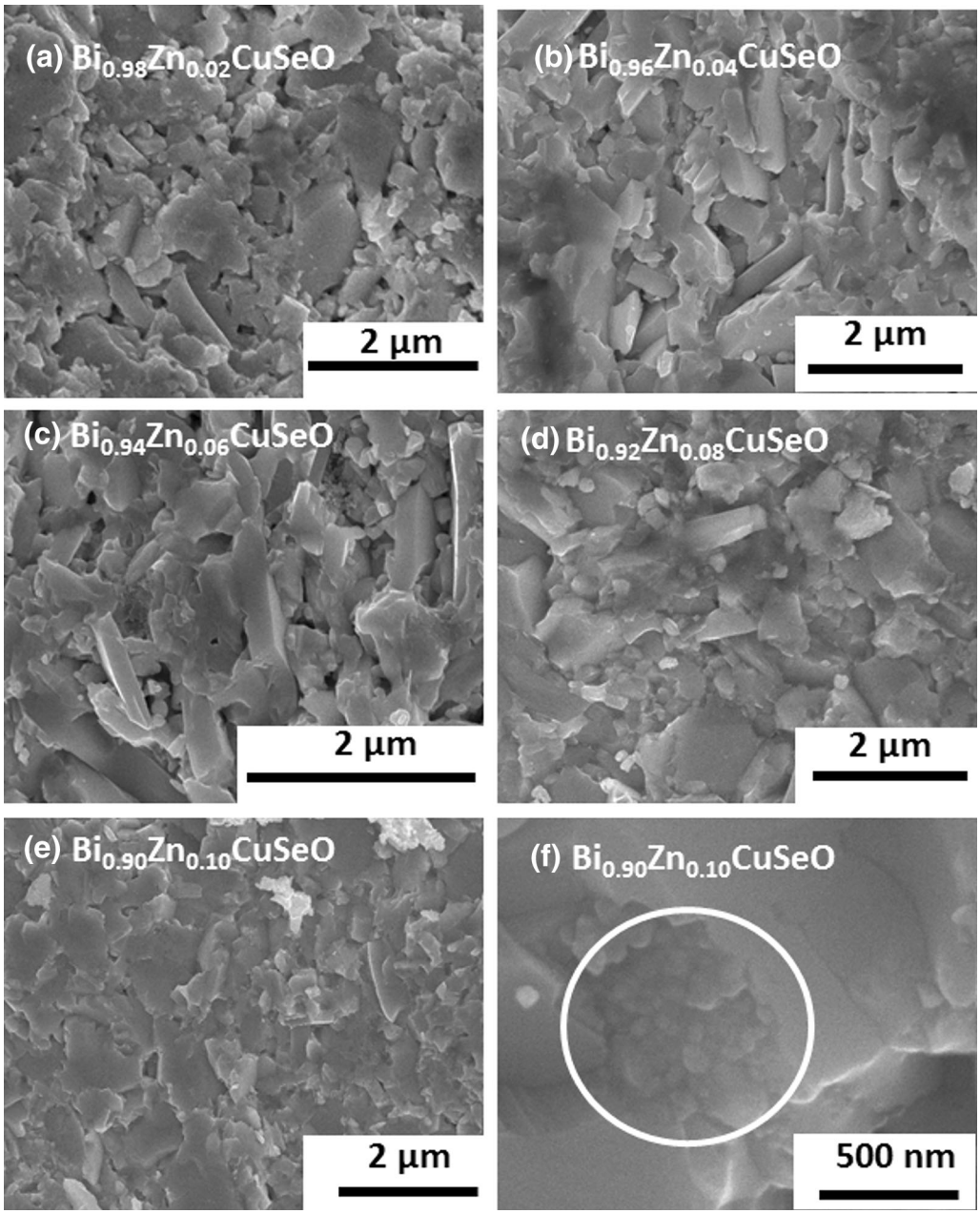

Fig. 5. Secondary electron (SE) image of the fractured surface of (a) $Bi_{0.98}Zn_{0.02}CuSeO$ (b) $Bi_{0.96}Zn_{0.04}CuSeO$ (c) $Bi_{0.94}Zn_{0.06}CuSeO$ (d) $Bi_{0.92}Zn_{0.08}CuSeO$ (e) $Bi_{0.90}Zn_{0.10}CuSeO$ (f) High-resolution image of $Bi_{0.90}Zn_{0.10}CuSeO$.

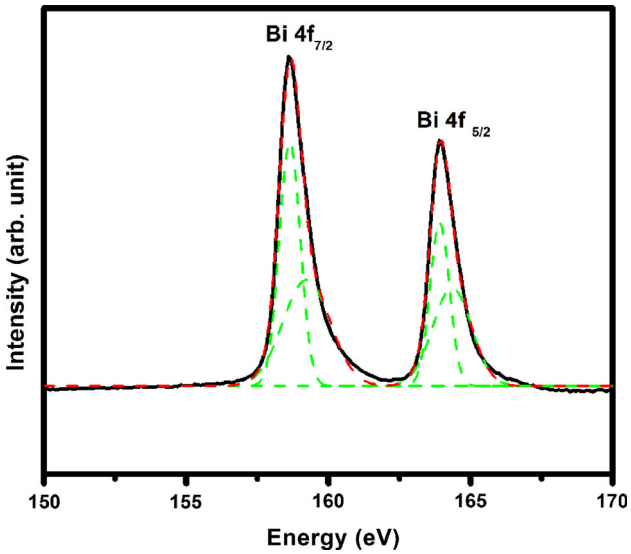

Fig. 6. The x-ray photo electron spectra of the Bi 4f state for the $Bi_{0.90}Zn_{0.10}CuSeO$ sample. The black solid line represents the experimental data. The green dashed line indicates the individual peaks. The red dashed line indicates the overall fit of the data (Color figure online).

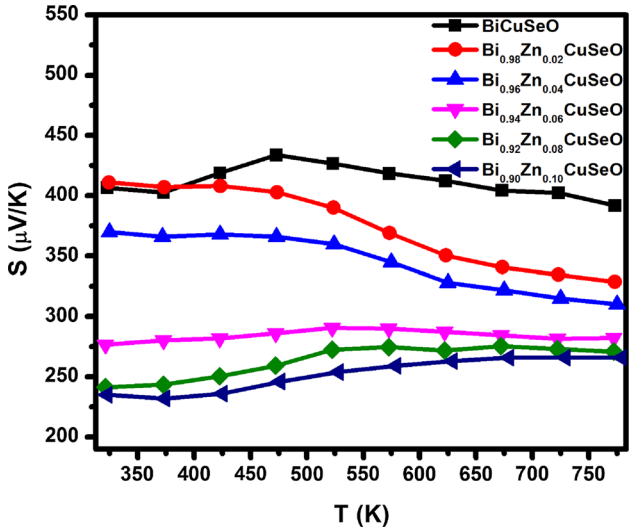

Fig. 7. The temperature dependence of Seebeck coefficient of the $Bi_{1-x}Zn_xCuSeO$ (x = 0.0, 0.02, 0.04, 0.06, 0.08 and 0.10) samples measured from 323 K to 773 K.

the C 1 s peak (284.8 eV[27]). Two different peaks due to the $4f^{7/2}$ and $4f^{5/2}$ occur because of the spin orbit coupling of the 4f electrons. The asymmetry in the peaks occur due to the convolution of multiple peaks. Each peak was fitted with two Gaussian peaks. The peaks at the 159.1 eV and 164.4 eV belong to the Bi^{+3} state.[27] The binding energy of the other two peaks are higher than that of the Bi^{+3} state at 159.7 eV and 164.9 eV, respectively. This essentially indicates that these peaks belong to a higher oxidation state of Bi. However, the binding energy of the peaks are lower than that of the Bi^{+5} state (160.3 eV and 165.3 eV respectively[27]) and belong to the Bi^{+4} state.[28]

Seebeck Coefficient (S)

The Seebeck coefficients of the samples are shown in Fig. 7. All the samples show positive Seebeck coefficients suggesting *p*-type conductivity. The Seebeck coefficient of the samples shows a decreasing trend with increasing doping percentage. This monotonic decrease in the Seebeck coefficient with doping is due to the increase in carrier concentration. The Seebeck coefficients of the samples $Bi_{0.94}Zn_{0.06}CuSeO$, $Bi_{0.92}Zn_{0.08}CuSeO$, and $Bi_{0.90}Zn_{0.10}CuSeO$ are temperature independent from 573 K to 773 K. This shows that the number and the entropy of the charge carriers do not depend on the temperature, but only on the doping concentration. This can be attributed to the hopping transport of small polarons. A polaron is a self-trapped localized electron/hole that is bound in the potential well produced by the displacement of neighboring atoms. This type of polaronic conduction is observed in many organic polymers as well as oxides.[29] The transition metal oxides are more likely to have this type of conduction because of the localization of carriers.[30] For example, $La_{1-x}Sr_xCrO_3$ has a temperature independent Seebeck coefficient of $\sim$ 600 μV/K for x = 0.02 and $\sim$ 200 μV/K for x = 0.20 in the temperature range of 300–450 K.[31] However, localized holes and hopping conduction is unusual in the BiCuSeO system. This is because the hole transport in BiCuSeO takes place by band conduction in the Cu_2Se_2 layer. For example, hole-dopants such as Pb,[11] Ca,[16] or Ba[18] at Bi site transfer holes to the Cu_2Se_2 layer and, therefore, these holes exhibit band conduction. A telltale signature of this hole transfer is an elongated *c*-axis due to charge redistribution and the subsequent weakened coulomb coupling between two layers. In this study, the *c*-axis did not change much on doping Zn. This implies that the charge is not transferred from the $(Bi_2O_2)^{+2}$ to the $(Cu_2Se_2)^{-2}$ layer; in other words, the holes are localized in the $(Bi_2O_2)^{+2}$ layer. The charge compensation mechanism could be due to the increase in the oxidation state of Bi to + 4 state from + 3 when Zn is doped at the Bi site as observed in the XPS results or anionic vacancies in the $(Bi_2O_2)^{+2}$ layer. This mechanism of charge compensation is also observed in Ca^{+2} doped BiCuSeO.[28] Where, the charge compensation due to Ca^{+2} doped at the Bi site is mediated by the increase in the valence state of Bi. The possible conduction pathway for these localized holes in the $(Bi_2O_2)^{+2}$ layer could be the Bi atoms. Although the valence band consists mostly of the Cu 3d and Se 4p states, weak Bi 6p x/y states present in the valence band can affect the band structure of BiCuSeO.[4] These states can accommodate the charge carriers in the Bi_2O_2 layer. Further, the ionic nature of the bonding between Bi and O results in strong electron–phonon coupling and favours the formation of small polarons.[32] For small polarons, entropy due to carriers is largely

determined by the configurational entropy of mixing for a fixed number of charge carriers. The high temperature Seebeck coefficient of small polarons is controlled by this entropy of mixing according to the formula

$$S = \frac{k_B}{e}\frac{\partial(\ln g)}{\partial N} \tag{2}$$

where k_B the Boltzmann constant, e is the charge of an electron, g is the number of configurations and $k_B \ln(g)$ is the configurational entropy. This gives rise to the Heikes formula $S = \frac{k_B}{e}\ln\frac{1-y}{y}$,[33] which describes the Seebeck coefficient of small polarons instead of Mott's formula.[34] For carriers with spin, the number of possible configurations (g) (accounting for both spin-up and spin-down holes) is

$$g = \sum_{N_i=0}^{N} \frac{N_A!}{N_i!(N_A - N_i)!} \times \frac{N_A!}{N_i!(N_A - N_i)!} \tag{3}$$

where N is the number of holes, N_A is the number of available sites, and N_i is the summation index. The Seebeck coefficient can be derived by simplifying Eq. 2:

$$S = \frac{k_B}{e}\ln\frac{(2-y)}{y} \tag{4}$$

where y is the ratio between N and N_A, that is, the ratio between the number of holes and the number of the available site for hopping. This is the modified Heikes formula for electrons/holes with spin, as given by Chaikin and Beni.[34] The Seebeck coefficient also includes the vibrational entropy part S^*, but it is neglected in general due to its low value of ≤ 10 μV/K.[34] For $Bi_{1-x}Zn_xCuSeO$, each Zn atom liberates one hole in the system according to the defect equation:

$$Bi_{1-x}Zn_xCuSeO \rightarrow Zn'_{Bi} + h^{\bullet} \tag{5}$$

Since the polarons hop from one Bi site to the other, the ratio y can be estimated as $y = \frac{\text{no. of holes}}{\text{no. of Bi sites}} = x/(1-x)$. Hence, the modified Heikes formula can be used to predict the Seebeck coefficient of the samples from 573 K to 773 K. The comparison between the Seebeck coefficient calculated from the modified Heikes formula and the average Seebeck coefficient measured from 573 K to 773 K is given in Table II. The calculated values are within ~ 18 μV/K of the observed values. The Seebeck coefficient of $Bi_{0.90}Zn_{0.10}CuSeO$ at 773 K is higher than that of band conductors like $Bi_{0.90}Ba_{0.10}CuSeO$ (~ 150 μV/K) and $Bi_{0.90}Ca_{0.10}CuSeO$ (~ 160 μV/K)[16] at the same temperature and doping percentage. This is because the Seebeck coefficient strongly decreases with increasing carrier concentration in the case of band conduction according to Mott's formula ($1/n^{2/3}$ dependence).[35]

The Seebeck coefficients of $Bi_{0.98}Zn_{0.02}CuSeO$ and $Bi_{0.96}Zn_{0.04}CuSeO$ decrease with temperature. This can be attributed to the fact that the holes arising from Cu vacancies have significant contribution in the carrier concentration. As a result, the overall Seebeck coefficient is not solely due to polarons, and hence, the Seebeck coefficient shows temperature dependence. The decreasing trend in the Seebeck coefficient with increasing temperature can be explained in terms of the activated behaviour of conduction. The conduction in the pristine sample is only due to Cu vacancies. The electrical resistivity reduces with increasing temperature for the pristine sample. This indicates that the holes can generate with increasing temperature for the Cu vacancies. This increasing charge carrier concentration decreases the Seebeck coefficient according to Mott's formula. As Cu vacancies also play a role in conduction for the sample with $x = 0.02$ and 0.04, this explains the monotonically decreasing Seebeck coefficient in those samples.

The possibility that Zn does not substitute at the Bi site may not be the case because this would essentially mean the vacancies of Bi will also be present in the system. Vacancies of Bi can severely reduce the Seebeck coefficient of BiCuSeO, which has been established both theoretically and experimentally[4,22]. For example, the Seebeck coefficient with a 4 at.% of Bi vacancy is < 100 μV/K at 323 K, while the Seebeck coefficient of the Zn-doped samples is much higher (~ 240 μV/K at 323 K for 10 at.% doping fraction). This further proves that the amount of Bi vacancies (if present in the system) is less, and the Bi sites are mostly occupied. This in turn proves that Zn is doped at the Bi site. Another possibility of introduction of holes in the system is Cu vacancies. The holes introduced in the BiCuSeO system due to the Cu vacancies are mobile holes, which can result in a temperature dependent Seebeck coefficient. This temperature dependence is absent in the case of $Bi_{0.94}Zn_{0.06}CuSeO$, $Bi_{0.92}Zn_{0.08}CuSeO$ and $Bi_{0.90}Zn_{0.10}CuSeO$ samples. This indicates that Cu vacancies do not have major contribution in the conduction for these samples.

Electrical Resistivity (ρ)

The electrical resistivity of the samples is shown in Fig. 8. The electrical resistivity of the pristine sample at 323 K is 3.76 mΩ m, which is less than the reported values ~ 10 mΩ m (~ 1 S/cm).[3] This can be attributed to the Cu vacancies, which can easily form in the system during synthesis.[3] The electrical resistivity monotonically decreases with increasing doping percentage. This shows that doping of Zn generates carriers according to the defect Eq. 5. The monotonic decrease of electrical resistivity with doping concentration agrees with the trend of the Seebeck coefficient and validates the fact that hole concentration increases with increasing doping concentration. It also proves that

Table II. Comparison of the average Seebeck coefficient from 573 K to 773 K and the value predicted by the modified Heikes formula

Sample	Average Seebeck coefficient from 573 K to 773 K (μV/K)	Seebeck coefficient from modified Heikes formula (μV/K)
$Bi_{0.94}Zn_{0.06}CuSeO$	286	304
$Bi_{0.92}Zn_{0.08}CuSeO$	273	281
$Bi_{0.90}Zn_{0.10}CuSeO$	262	263

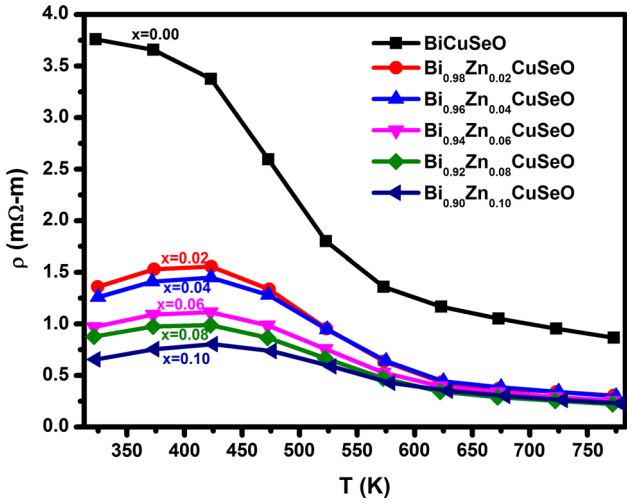

Fig. 8. The temperature dependence of electrical resistivity of the $Bi_{1-x}Zn_xCuSeO$ (x = 0.0, 0.02, 0.04, 0.06, 0.08 and 0.10) samples from 373 K to 773 K.

Zn is doped at the Bi site. The lowest electrical resistivity of 0.23 mΩ m was obtained for $Bi_{0.90}Zn_{0.10}CuSeO$ at 773 K. This value is much higher than that of the Ba ($\sim$ 0.057 mΩ m) or Ca ($\sim$ 0.05 mΩ m) doped BiCuSeO at the same temperature and doping concentration.[16,18] The electrical resistivity of all the doped samples first increased with temperature till 423 K, showing a metallic behaviour followed by a decrease. This behaviour is shown by many transition metal doped BiCuSeO (at the Bi site) at low concentration, for example in Cd ($<$ 5 at.%),[20] and Ag ($\leq$ 10 at.%).[36] The behaviour can be explained in the following manner: the resistivity increases with increasing temperature until 423 K because of the charge carrier-phonon scattering, which increases with increasing temperature. The transition from band conduction to polaronic conduction occurs when the width of the polaron band is comparable to the energy fluctuation of scattering. The energy fluctuation due to scattering increases with increasing temperature as a result of the transition from band conduction to polaronic conduction that takes place above a certain temperature.[37] The conduction of small

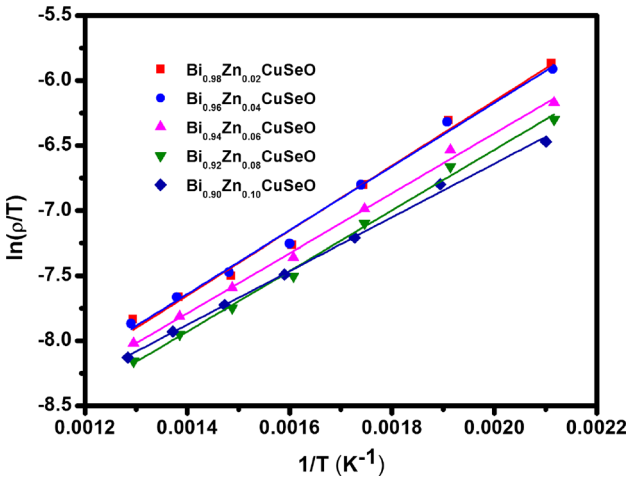

Fig. 9. Electrical resistivity of the $Bi_{1-x}Zn_xCuSeO$(x = 0.0, 0.02, 0.04, 0.06, 0.08 and 0.10) samples fitted with the small polaron hopping model.

polarons is characterized by a constant carrier density along with the activated behaviour of drift mobility. The drift mobility of small polarons is thermally activated and increases with temperature. This activated behaviour of the mobility reduces the electrical resistivity with increasing temperature. As a result, the electrical resistivity increases until the onset of polaronic conduction, followed by a decrease with rising temperature. The electrical resistivity of the doped samples from 473 K to 773 K was fitted with the small polaron hopping model as shown in Fig. 9 with the equation:

$$\rho = \rho_0 T \exp\left(\frac{E_A}{k_B T}\right) \quad (6)$$

where ρ_0 is a constant, T is the absolute temperature and E_A is the activation energy of the polarons. Since the conduction in $Bi_{0.98}Zn_{0.02}CuSeO$ and $Bi_{0.96}Zn_{0.04}CuSeO$ is due to both polarons and holes, the goodness of fit was not as good as in other samples, where conduction is mainly due to small polarons only (the goodness of fit is given in supplementary table SII). The activation energies of the $Bi_{0.94}Zn_{0.06}CuSeO$, $Bi_{0.92}Zn_{0.08}CuSeO$ and $Bi_{0.90}Zn_{0.10}CuSeO$ were 0.20, 0.20 and 0.18 eV, respectively (see supplementary table SII). These values are of the same order compared to different oxides, for example, 0.16 eV for $LaCoO_3$.[38] In $LaMn_{1-x}Fe_xO_3$ the activation varies from 0.125 eV for x = 0.125 to 0.249 eV for x = 0.6.[39] The activation energy depends on the disorder potential W_D and the hopping energy of the small polaron W_H, by the relation $E_A = W_H + W_D/2$.[33] The pre-exponential factor depends on the doping concentration, optical phonon frequency and inter-site distance. There is not much variation in both the activation energy and the pre exponential factor (see supplementary table SII) with doping probably because doping fraction of the samples are close to each

other (6 at.%, 8 at.% and 10 at.%). Below the onset of the polaronic conduction, the charge carrier behaves as band conductor but with increased effective mass $m_p = m^* e^{\gamma}$, where m^* is the effective mass corresponding to the rigid lattice and γ is a constant (≥ 3).[30] This increased effective mass of the charge carriers decreases its mobility.

Power Factor (S^2/ρ)

The power factor (S^2/ρ) of the samples is shown in Fig. 10. The power factor of the doped samples first decreases with increasing temperature from 323 K to 423 K and then increases until 773 K. This is mainly because of the transition of resistivity at 423 K. The highest power factor of 0.35 mW/m K^2 was obtained for $Bi_{0.98}Zn_{0.02}CuSeO$ sample at 773 K, which is almost twice that of the pristine sample (0.18 mW/m K^2) at the same temperature. This value is lower than the Pb ($\sim$ 0.8 mW/m K^2)[11] Ba ($\sim$ 0.62 mW/m K^2)[18] and Ca-doped ($\sim$ 0.65 mW/m K^2)[16] BiCuSeO, but higher than the Mg doped BiCuSeO ($\sim$ 0.2 mW/m K^2)[15] at 773 K. Even though Zn has a high solubility at the Bi site, the highest power factor has been obtained for the lowest doping percentage (2%) in this study. In general, the power factor of the hole-doped BiCuSeO is optimized at a carrier concentration around $1 \times 10^{21}/cm^3$.[3] In this report, the polarons are responsible for electrical conduction in the $Bi_{0.94}Zn_{0.06}CuSeO$, $Bi_{0.92}Zn_{0.08}CuSeO$ and $Bi_{0.90}Zn_{0.10}CuSeO$ samples while both holes and small polarons are accountable for the same in the $Bi_{0.98}Zn_{0.02}CuSeO$ and $Bi_{0.96}Zn_{0.04}CuSeO$ samples. In general, small polarons, have very low mobility (< 1 cm^2/V s) compared to holes.[33] This mobility of polarons is much lower compared to even in heavily doped BiCuSeO, such as ~ 3 cm^2/V s $Bi_{0.875}Ba_{0.125}CuSeO$[18] and ~ 2.5 cm^2/V s in $Bi_{0.90}Ca_{0.10}CuSeO$.[16] This, along with the localization of charge carriers lowers the electrical resistivity in comparison to band conduction of holes. In turn, this adversely affects the power factor of the samples with small polarons as charge carriers. Since $Bi_{0.98}Zn_{0.02}CuSeO$ has holes as well as small polarons as the charge carriers, the mobility does not deteriorate as much as the rest of the samples, and as a result, the power factor of this sample is maximum.

AC Conductivity

In order to confirm the hopping conductivity, the ac conductivity investigation was carried out for the $Bi_{0.90}Zn_{0.10}CuSeO$ sample in a temperature interval of 300 K to 500 K, as shown in Fig. 11a. The frequency variation of ac conductivity at selected temperatures (300 K and 500 K) are presented in Fig. 11b. The measured frequency window is characterized by two distinct regions: one plateau and one dispersion regime, due to the effects of grain interior. For room temperature ($T \sim 300$ K), we have named these two regions as region I and region II (Fig. 11b). In region I (i.e., $\leq 10^4$ Hz), the plateau represents the total conductivity followed by a plateau region in which ac conductivity of the sample is independent of frequency. In region II (i.e., 10^4–10^6 Hz) the dispersion region represents the grains interior contribution to the total conductivity. With the increase in temperature, the frequency dispersion region gradually moves towards the higher frequency range. To understand ac conductivity dynamics, the total conductivity of the localized charge carriers can be explained by Jonscher's power law[40]:

$$\sigma(\omega) = \sigma_0 + A\omega^n \qquad (7)$$

where σ_0 is the frequency independent conductivity, i.e., dc conductivity (σ_{dc}), the coefficient A and the exponent n ($0 \leq n \leq 1$) are the temperature and

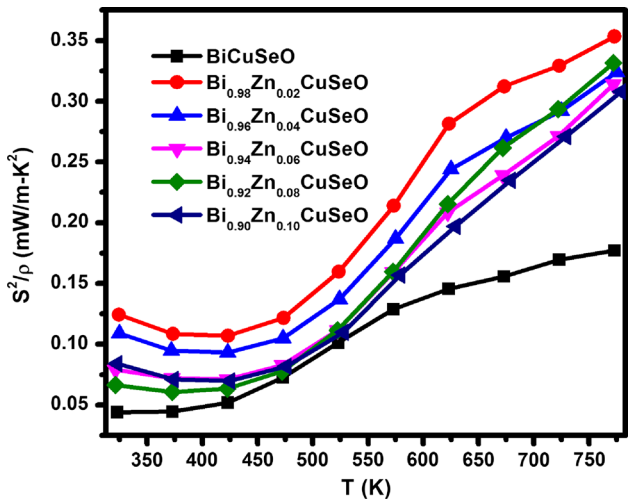

Fig. 10. Power factor (S^2/ρ) of the $Bi_{1-x}Zn_xCuSeO$ (x = 0.0, 0.02, 0.04, 0.06, 0.08 and 0.10) samples as a function of temperature from 323 K to 773 K.

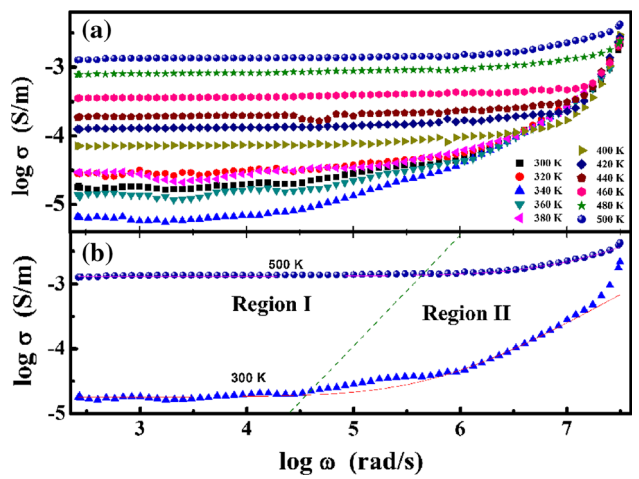

Fig. 11. Frequency dependence of the ac conductivity of the $Bi_{0.90}Zn_{0.10}CuSeO$ sample (a) at various temperatures, (b) the fitted experimental data with the power law for temperatures 300 K and 500 K.

material geometry-dependent parameters. The experimental conductivity data are fitted by Eq. 7 for the two different temperatures 300 K and 500 K as shown in Fig. 11b, whereas the value of n for region II (10^4 to 10^6 Hz) is found to be 0.91 and 0.85 for 300 K and 500 K, respectively. This frequency dependent conductivity is due to the hopping conductivity,[41] and the value of n close to unity indicates that there is lattice response to the conductivity.[40]

Figure 12a shows the frequency dependent dielectric constant (ε') in the temperature range from 300 K to 500 K. These plots show that there is only one Debye-like dispersion in the whole measured frequency range. With the increase of temperature, the dispersion region move towards the higher frequency regime. At low frequency, the permanent dipoles align themselves along the field and contribute fully to the total polarization of the dielectric. At higher frequencies, the variation in the field is too rapid for the dipoles to align themselves so their contributions to the polarization and hence to dielectric permittivity can become negligible resulting in a decrease of the dielectric constant ε' with increasing frequency.

Figure 12b shows frequency dependence of tanδ in the temperature range 300–500 K. It is found that relaxation peaks are observed in the measured frequency range, which is due to the presence of grains only. In the measured temperature range, it is found that all the loss tangent peaks move towards higher frequency side with the increase in temperature. Rudimentarily, the loss tangent peak depends on the mobility of charge carriers and the temperature.[42] The mobility of the charge carriers increases with temperature and commence to relax at higher frequency side, which results in the mechanism of the loss tangent peak towards higher frequency side. Similarly, the loss peaks for grains are visible above 10^4 Hz (logω = 4.0) which shift towards the higher frequency side and move out of the measured frequency range at high temperatures. The value of the tangent loss for grains is found around 0.5 at frequencies above 10^4 Hz. The observed value of tangent loss for grains is related to the number of dipoles available for relaxation process and the charge carrier mobility.[43,44] With the increase in temperature, both ε' dispersion regions (Fig. 12a) and tanδ peaks (Fig. 12b) move towards higher frequency side, which suggests the thermally activated behavior of the relaxation process. Thus, the impedance spectroscopy confirms the hopping conductivity of the charge carriers, and it also confirms that mobility of the charge carriers increase with temperature.

Thermal Conductivity (κ)

The total thermal conductivities of the samples are shown in Fig. 13. The thermal conductivity decreases with increasing temperature. The electronic part of the thermal conductivity (κ_e) was calculated from the Wiedemann–Franz relation

$$\kappa_e = \frac{LT}{\rho} \tag{8}$$

where L is the Lorenz number. There are very few reports on the Lorenz number of small polarons. Lee et al. pointed out that the Lorenz number of degenerate small polarons is equal to the degenerate limit of normal broad band semiconductors ($L_0 = 2.44 \times 10^{-8}$ WΩ/K^2). On the other hand, the Lorenz number of non-degenerate small polaron is $\approx L_0/6 \approx 0.41 \times 10^{-8}$ WΩ/K^2. In the intermediate case between degenerate and non-degenerate small polarons, the Lorenz number can vary significantly between both limits at non-zero temperatures.[45] In this paper, the Lorenz number was taken as

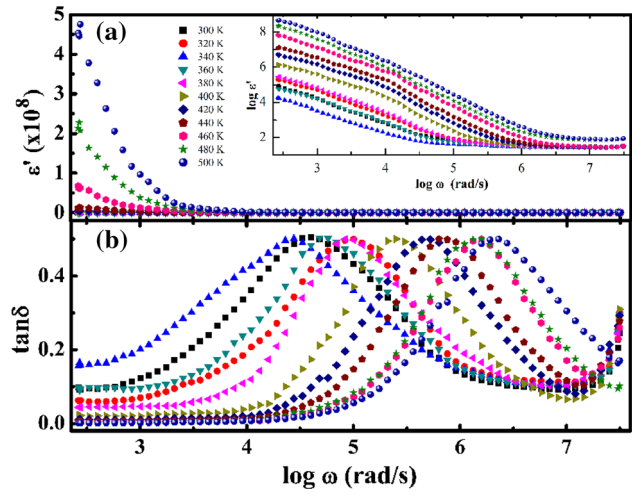

Fig. 12. Frequency dependence of (a) ε' and (b) tanδ at various temperatures for the $Bi_{0.90}Zn_{0.10}CuSeO$ sample. Inset of (a) shows the logε' versus logω plot.

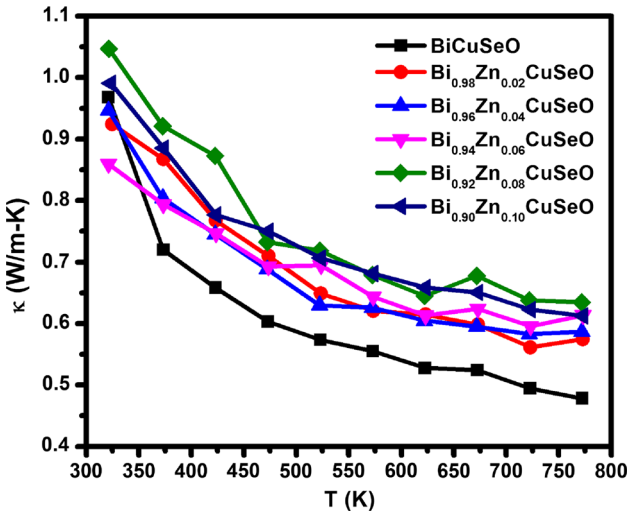

Fig. 13. The temperature dependence of thermal conductivity of the $Bi_{1-x}Zn_xCuSeO$ (x = 0.0, 0.02, 0.04, 0.06, 0.08 and 0.10) samples measured from room 323 K to 773 K.

1.5×10^{-8} WΩ/K^2 following the report of Zhou et al. on the small polaron conductor $La_{1-x}Sr_xCoO_3$.[46] The lattice part of the thermal conductivity was calculated by subtracting the electronic part from the total thermal conductivity as shown in Fig. 14. The electronic part of the thermal conductivity is low compared to the lattice part of the thermal conductivity. The lattice thermal conductivity decreases with increasing temperature due to the phonon–phonon Umklapp scattering at high temperatures. The lattice thermal conductivity of the pristine sample was low (< 1 W/m–K) throughout the temperature range. This low lattice thermal conductivity of the sample is related to the high atomic displacement of Cu, the interlayer scattering of phonons and the high Gruneisen parameter of 1.5.[47] The trend of the lattice thermal conductivity of the doped samples cannot be ascertained because of the speculative Lorenz number. Despite heavy mass fluctuation scattering, the lattice thermal conductivity of the doped samples is higher than that of the pristine sample even if the degenerate limit of the Lorenz number is taken for calculating the electronic thermal conductivity. This increase could be related to the increase in the bond strength due to the substitution of Zn. Unlike other metals, 3d transition metals favour covalent bonding with O.[48] In general, covalent bonds have higher strength than ionic bonds. This may lead to higher thermal conductivity in the doped samples. Similarly, another 3d transition metal—Ni-doped at the Bi site of BiCuSeO, has shown a similar increasing trend in thermal conductivity with increasing doping percentage.

Dimensionless Figure of Merit (zT)

The zT of the samples is depicted in Fig. 15. The maximum zT of 0.48 was achieved for the $Bi_{0.98}Zn_{0.02}CuSeO$ sample at 773 K, which is 65% higher than that of the pristine sample at the same temperature. This is mainly due to the increased power factor of $Bi_{0.98}Zn_{0.02}CuSeO$ in comparison with the pristine sample. However, the increment in the power factor is not translated in the zT due to the increased thermal conductivity of the sample. Although this value of zT is not as high as in the case of some successful dopants such as Pb (∼ 1.10 at 773 K for 6 at.% doping) or Ba (∼ 0.95 at 773 K for 12 at.% doping), in BiCuSeO it is higher than the Ni-doped BiCuSeO (∼ 0.25 at 773 K) for 0.04 at.%[19] and Mg-doped BiCuSeO (∼ 0.37 at 773 K) for 0.125 at.% doping.

CONCLUSIONS

$Bi_{1-x}Zn_xCuSeO$ (x = 0, 0.02, 0.04, 0.06, 0.08 and 0.10) has been successfully synthesized by solid state reaction, using zinc oxide as the source of zinc. The doping of Zn at the Cu site was prevented by using ZnO as the precursor instead of Zn. All the peaks in the XRD pattern of the samples were indexed to BiCuSeO, confirming the crystal structure and phase purity of the samples. This phase purity is due to the high solubility of Zn at the Bi site of BiCuSeO. The coexistence of + 3 and + 4 oxidation state of Bi was confirmed by XPS for the $Bi_{0.90}Zn_{0.10}CuSeO$ sample, which can account for the charge compensation due to Zn doping. The Seebeck coefficient and electrical resistivity monotonically decrease with increasing doping percentage, which indicates an increase in the carrier concentration due to increasing Zn_{Bi} defects. The Seebeck coefficients of the $Bi_{0.94}Zn_{0.06}CuSeO$, $Bi_{0.92}Zn_{0.08}CuSeO$ and $Bi_{0.90}Zn_{0.10}CuSeO$ samples are temperature independent above 573 K and agree

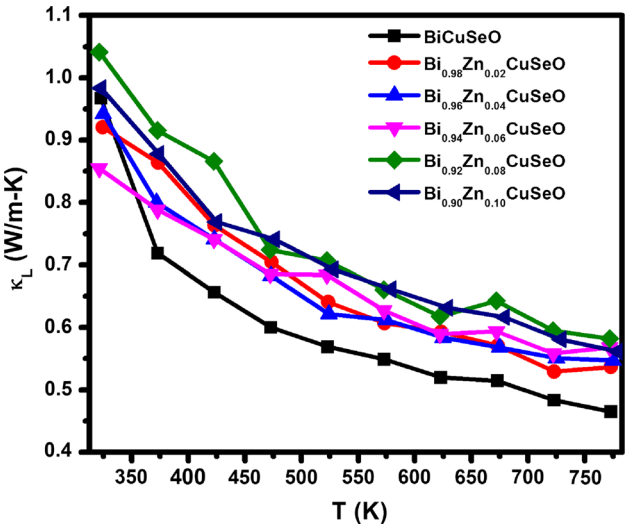

Fig. 14. Lattice thermal conductivity of the $Bi_{1-x}Zn_xCuSeO$ (x = 0.0, 0.02, 0.04, 0.06, 0.08 and 0.10) samples as a function of temperature from 373 K to 773 K.

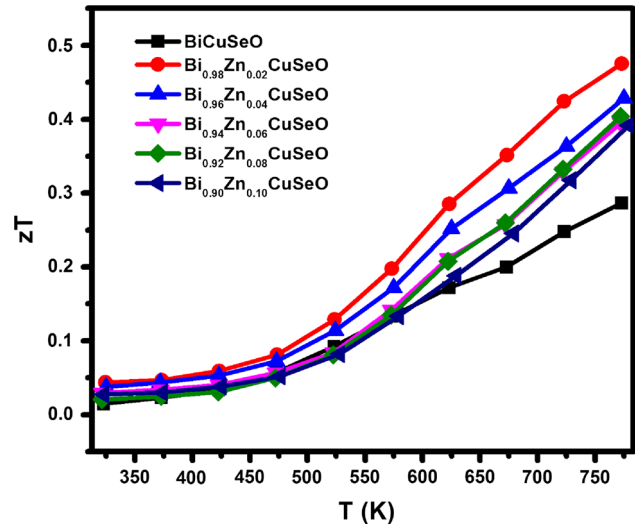

Fig. 15. Dimensionless figure of merit of the $Bi_{1-x}Zn_xCuSeO$ (x = 0.0, 0.02, 0.04, 0.06, 0.08 and 0.10) samples (zT) of the samples as a function of temperature from 373 K to 773 K.

with the modified Heikes formula. This temperature independence could be because of small polaron hopping from one Bi atom to the other Bi atom. The transition in electrical resistivity at 423 K can also be explained by the activated drift mobility of the small polarons. The increase in the mobility with temperature as well the hopping conductivity was confirmed by impedance spectroscopy. The highest power factor of 0.35 mW/m K^2 was obtained for the $Bi_{0.98}Zn_{0.02}$ CuSeO sample, which is two times higher than that of the pristine sample. This increment in the power factor could not be retained in zT mainly because of the increased thermal conductivity in the doped samples.

ACKNOWLEDGMENTS

We would like to thank Ms. Shriparna Mukherjee for measuring the Seebeck coefficientand electrical resistivity and Prof. Kamanio Chattopadhyay for providing the facility. We would also like to thank the Supercomputer Education and Research Centre (SERC) for providing the computational facility. One of the authors, Sayan Das, would like to thank the Council of Scientific and Industrial Research (CSIR) for providing a scholarship.

ELECTRONIC SUPPLEMENTARY MATERIAL

The online version of this article (https://doi.org/10.1007/s11664-019-07118-5) contains supplementary material, which is available to authorized users.

REFERENCES

1. L.-D. Zhao, S.-H. Lo, Y. Zhang, H. Sun, G. Tan, C. Uher, C. Wolverton, V.P. Dravid, and M.G. Kanatzidis, *Nature* 508, 373 (2014).
2. A.T. Duong, V.Q. Nguyen, G. Duvjir, V.T. Duong, S. Kwon, J.Y. Song, J.K. Lee, J.E. Lee, S. Park, T. Min, J. Lee, J. Kim, and S. Cho, *Nat. Commun.* 7, 13713 (2016).
3. L.D. Zhao, J. He, D. Berardan, Y. Lin, J.F. Li, C.W. Nan, and N. Dragoe, *Energy Environ. Sci.* 7, 2900 (2014).
4. C. Lee, T.-H. An, E.E. Gordon, H.S. Ji, C. Park, J.-H. Shim, Y.S. Lim, and M.-H. Whangbo, *Chem. Mater.* 29, 2348 (2017).
5. F. Li, J.F. Li, L.D. Zhao, K. Xiang, Y. Liu, B.P. Zhang, Y.H. Lin, C.W. Nan, and H.M. Zhu, *Energy Environ. Sci.* 5, 7188 (2012).
6. B. Feng, G. Li, Y. Hou, C. Zhang, C. Jiang, J. Hu, Q. Xiang, Y. Li, Z. He, and X. Fan, *J. Alloys Compd.* 712, 386 (2017).
7. Y. Liu, J. Lan, W. Xu, Y. Liu, Y.L. Pei, B. Cheng, D.B. Liu, Y.H. Lin, and L.D. Zhao, *Chem. Commun.* 49, 8075 (2013).
8. Y.L. Pei, H. Wu, D. Wu, F. Zheng, and J. He, *J. Am. Chem. Soc.* 136, 13902 (2014).
9. J. Sui, J. Li, J. He, Y.-L. Pei, D. Berardan, H. Wu, N. Dragoe, W. Cai, and L.-D. Zhao, *Energy Environ. Sci.* 6, 2916 (2013).
10. Z. Li, C. Xiao, S. Fan, Y. Deng, W. Zhang, B. Ye, and Y. Xie, *J. Am. Chem. Soc.* 137, 6587 (2015).
11. J. Le Lan, Y.C. Liu, B. Zhan, Y.H. Lin, B. Zhang, X. Yuan, W. Zhang, W. Xu, and C.W. Nan, *Adv. Mater.* 25, 5086 (2013).
12. J. Li, J. Sui, Y. Pei, X. Meng, D. Berardan, N. Dragoe, W. Cai, and L.D. Zhao, *J. Mater. Chem. A* 2, 4903 (2014).
13. D. Sun Lee, T.H. An, M. Jeong, H.S. Choi, Y. Soo Lim, W.S. Seo, C.H. Park, and C. Park, Park HH. *Appl. Phys. Lett.* 103, 232110 (2013).
14. A. Achour, K. Chen, M.J. Reece, and Z. Huang, *J. Alloys Compd.* 735, 861 (2018).
15. J. Li, J. Sui, C. Barreteau, D. Berardan, N. Dragoe, W. Cai, Y. Pei, and L.D. Zhao, *J. Alloys Compd.* 551, 649 (2013).
16. Y.-L. Pei, J. He, J.-F. Li, F. Li, Q. Liu, W. Pan, C. Barreteau, D. Berardan, N. Dragoe, and L.-D. Zhao, *NPG Asia Mater.* 5, e47 (2013).
17. C. Barreteau, D. Bérardan, E. Amzallag, L. Zhao, and N. Dragoe, *Chem. Mater.* 24, 3168 (2012).
18. J. Li, J. Sui, Y. Pei, C. Barreteau, D. Berardan, N. Dragoe, W. Cai, J. He, and L.D. Zhao, *Energy Environ. Sci.* 5, 8543 (2012).
19. Y.C. Liu, J.F. Liu, B.P. Zhang, and Y.H. Lin, *Key Eng. Mater.* 3, 602 (2014).
20. M.U. Farooq, S. Butt, K. Gao, Y. Zhu, X. Sun, X. Pang, S.U. Khan, F. Mohmed, A. Mahmood, N. Mahmood, and W. Xu, *RSC Adv.* 6, 33789 (2016).
21. N. Samaele, P. Amornpitoksuk, and S. Suwanboon, *Powder Technol.* 203, 243 (2010).
22. S. Das, A. Ramakrishnan, K.H. Chen, D.K. Misra, and R.C. Mallik, *J. Phys. D Appl. Phys.* 51, 35501 (2018).
23. J. Rodríguez-Carvajal, *Phys. B Phys. Condens. Matter* 192, 55 (1993).
24. S. Das, R. Chetty, K. Wojciechowski, S. Suwas, and R.C. Mallik, *Appl. Surf. Sci.* 418, 238 (2017).
25. F.K. Lotgering, *J. Inorg. Nucl. Chem.* 9, 113 (1959).
26. S. Kumar and U. Schwingenschlogl, *Phys. Chem. Chem. Phys.* 18, 19158 (2016).
27. H. Fan, G. Wang, and L. Hu, *Solid State Sci.* 11, 2065 (2009).
28. C.L. Hsiao and X. Qi, *Acta Mater.* 102, 88 (2016).
29. B. Hartenstein, H. Bässler, S. Heun, P. Borsenberger, M. Van der Auweraer, and F.C. De Schryver, *Chem. Phys.* 191, 321 (1995).
30. I.G. Austin and N.F. Mott, *Science (80-.)* 168, 71 (1970).
31. D.P. Karim and A.T. Aldred, *Phys. Rev. B* 20, 2255 (1979).
32. T.D. Lee, F.E. Low, and D. Pines, *Phys. Rev.* 90, 297 (1953).
33. I.G. Austin and N.F. Mott, *Adv. Phys.* 18, 41 (1969).
34. P.M. Chaikin and G. Beni, *Phys. Rev. B* 13, 647 (1976).
35. M. Cutler, J.F. Leavy, and R.L. Fitzpatrick, *Phys. Rev.* 133, A1143 (1964).
36. Y. Liu, Y. Zheng, B. Zhan, K. Chen, S. Butt, B. Zhang, and Y. Lin, *J. Eur. Ceram. Soc.* 35, 845 (2015).
37. J. Hoffmann, P. Moschkau, S. Mildner, J. Norpoth, C. Jooss, L. Wu, and Y. Zhu, *Mater. Res. Express* 1, 046403 (2014).
38. E. Iguchi, K. Ueda, and W.H. Jung, *Phys. Rev. B* 54, 17431 (1996).
39. W. Khan, A.H. Naqvi, M. Gupta, S. Husain, and R. Kumar, *J. Chem. Phys.* 135, 054501 (2011).
40. A.K. Jonscher, *Nature* 267, 673 (1977).
41. S. Sen and R.N.P. Choudhary, *Mater. Chem. Phys.* 87, 256 (2004).
42. R. Tripathi, A. Kumar, and T.P. Sinha, *Pramana* 72, 969 (2009).
43. J. Liu, C.-G. Duan, W.-G. Yin, W.N. Mei, R.W. Smith, and J.R. Hardy, *Phys. Rev. B* 70, 144106 (2004).
44. E. Iguchi, N. Kubota, T. Nakamori, N. Yamamoto, and K.J. Lee, *Phys. Rev. B* 43, 8646 (1991).
45. K.K. Lee, A.S. Alexandrov, and W.Y. Liang, *Eur. Phys. J. B Condens. Matter Complex Syst.* 39, 459 (2004).
46. A.J. Zhou, T.J. Zhu, X.B. Zhao, H.Y. Chen, and E. Müller, *J. Alloys Compd.* 449, 105 (2008).
47. P. Vaqueiro, R.A.R. Al Orabi, S.D.N. Luu, G. Guelou, A.V. Powell, R.I. Smith, J.-P.P. Song, D. Wee, M. Fornari, G. Guélou, A.V. Powell, R.I. Smith, J.-P. P. Song, D. Wee, and M. Fornari, *Phys. Chem. Chem. Phys.* 17, 31735 (2015).
48. J. Owen and J.H.M. Thornley, Reports. *Prog. Phys.* 29, 675 (1966).